Photothermal Heating Enabled by Plasmonic Nanostructures for Electrokinetic Manipulation and Sorting of Particles

Justus Chukwunonso Ndukaife,[†,§] Avanish Mishra,[‡] Urcan Guler,[†] Agbai George Agwu Nnanna,[§] Steven T. Wereley,[‡] and Alexandra Boltasseva[*,†,⊥]

[†]School of Electrical & Computer Engineering and Birck Nanotechnology Center, Purdue University, West Lafayette, Indiana 47907, United States, [‡]School of Mechanical Engineering and Birck Nanotechnology Center, Purdue University, West Lafayette, Indiana 47907, United States, [§]Water Institute, Purdue University Calumet, Hammond, Indiana 46323, United States, and [⊥]DTU Fotonik, Department of Photonics Engineering, Technical University of Denmark, Lyngby, DK-2800, Denmark

ABSTRACT Plasmonic nanostructures support strong electromagnetic field enhancement or optical "hot spots" that are accompanied by local heat generation. This heating effect is generally seen as an obstacle to stable trapping of particles on a plasmonic substrate. In this work, instead of treating the heating effect as a hindrance, we utilized the collective photoinduced heating of the nanostructure array for high-throughput trapping of particles on a plasmonic nanostructured substrate. The photoinduced heating of the nanostructures is combined with an ac electric field of less than 100 kHz, which results in creation of a strong electrothermal microfluidic flow. This flow rapidly transports suspended particles toward the plasmonic substrate, where they are captured by local electric field effects. This work is envisioned to have application in biosensing and surface-enhanced spectroscopies such as SERS.

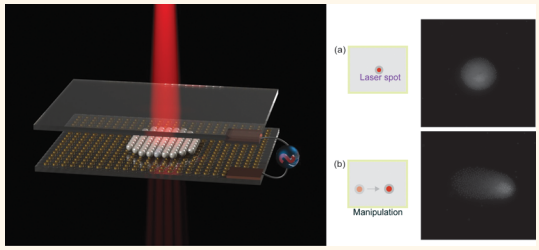

KEYWORDS: LSPR · plasmonic heating · photothermal effect · particle sorting · SERS · electrokinetics

The ability to trap particles by light using optical tweezers has generated a lot of interest within the past four decades.[1] In an optical tweezer, a tightly focused laser beam creates a strong optical gradient force for confining microparticles. Because of the diffraction limit, light can only be focused down to about half the wavelength in a medium, thus setting a limit on maximum achievable optical gradient force for a given laser power. Since the optical gradient force scales as the particle radius to the third power (in the quasi-static limit),[2] coupled with increased Brownian motion, it becomes difficult to address submicrometer and nanoscale objects with optical tweezers. As a result, plasmonic trapping, also known as plasmonic nanotweezing, is now actively investigated to overcome the limitations of optical tweezers. In conventional plasmonic tweezers, the local field enhancement generated *via* resonant coupling of incident photons with free electrons on metallic nanostructures is used to achieve subwavelength electromagnetic field confinement. This field, which is highly confined to the surface of the nanostructures, creates strong optical gradient forces, thus offering a route for trapping submicrometer and nanoscale particles.[3−6] Additionally, the highly localized and enhanced electromagnetic field, also known as "optical hot spots", can be engineered to create arbitrary optical trapping potential wells for confining particles.[7] However, the excitation of local field enhancement at plasmonic resonance is also accompanied by resonant light absorption, which results in local heat generation within the volume of the plasmonic nanostructures.[8,9] In the context of plasmonic trapping, generally the focus is on the enhanced local fields, while little attention is paid to the associated local heat generation or thermal hot spots. This local heating effect has been seen as an obstacle to stable trapping of particles on a plasmonic substrate because of heating-induced thermophoresis, convection, and even boiling.[6]

* Address correspondence to aeb@purdue.edu.

Received for review April 27, 2014 and accepted August 21, 2014.

Published online August 21, 2014
10.1021/nn502294w

© 2014 American Chemical Society

All these effects obscure the trapping process. Hence efforts have been made to suppress the heating effect by integrating a heat sink to dissipate excess heat[6] or by off-resonance excitation to minimize light absorption.[10] However, the emerging field of thermoplasmonics has identified the unique attribute of this heating effect for realization of nanoscale heat sources that can be remotely controlled and switched by light. Several applications harnessing this effect are being explored, including plasmonic photothermal therapy for destruction of tumor cells, photothermal imaging, and solar-powered steam generation.[11,12] Similar to the above-mentioned applications, which rely on a local heating effect enabled by resonantly excited plasmonic nanoparticles, this intrinsic heating effect could be harnessed for trapping, concentrating, manipulating, and sorting of micro- and nanoscale particles on a plasmonic substrate. Additionally, it is important to emphasize that suppressing the heating effect as in ref 6 leaves the enhanced electromagnetic field as the only photoinduced signal, which presents some practical challenges for plasmonic nanotweezers. First, because the enhanced electromagnetic field exists in the near-field, it produces only short-range interactions. Thus, the force field due to the optical hot spots can be felt only by an object after it has diffused to a distance several nanometers from the resonant nanostructure.[13] Since the transport of the object *via* Brownian motion is inherently very slow, only particles sufficiently close to the resonantly excited nanostructures can be trapped in a reasonable time frame. In addition, because the field is confined to the nanostructures, manipulating the laser source from one point to another effectively switches off the optical hot spots at the initial location and switches it on at another location. Now if the separation between the plasmonic nanostructures (*i.e.*, the trapping sites) is large such that near-field electromagnetic coupling is absent, then a trapped object cannot be manipulated by optical gradient forces (from near-field enhancement), as these are short-range interactions. Hence, transport of target particles over a long distance, which is important for varieties of lab-on-a-chip applications such as on-chip sorting, has not been shown using plasmonic nanotweezers.[14] These important issues suggest that there is a need for further advancement of plasmonic nanotweezer design.

It is important to emphasize that the use of a plasmonic substrate for particle trapping opens up additional applications beyond trapping of submicrometer and nanoscale particles. These include biosensing (for example *via* LSPR resonance shifts),[15,16] surface-enhanced spectroscopies,[17,18] and enhancing the radiative properties of emitters.[19] In biosensors for example, rapid transport and concentration of analytes are critical for reducing the detection time as well as improving the detection limit. Hence the ability to rapidly manipulate and sort micro- and nanoparticles on a plasmonic nanostructured substrate would greatly enable several lab-on-a-chip applications with plasmonic nanostructures. However, these applications have been hampered so far because of the diffusion-limited transport of particles to the trapping sites. Here instead of suppressing the photoinduced heating of a plasmonic nanoparticle array, we propose a way to take advantage of it for addressing the issue of dynamic transport of dielectric particles over long distance on plasmonic nanostructures. We demonstrate rapid particle transport, high-throughput concentration, and dynamic manipulation of micro- and nanoscale particles on a plasmonic nanostructured substrate, by harnessing the collective heating effect of an array of plasmonic nanostructures.

Our approach for the first time synergizes localized surface plasmon resonance with an optically induced electrokinetic phenomenon known as rapid electrokinetic patterning (REP), which achieves particle concentration by heating an electrode having an absorbing film with a tightly focused laser beam and a low-frequency ac electrokinetic phenomenon.[20,21] Here we have replaced a thin absorbing film substrate with plasmonic resonant nanostructures and harnessed the collective heating of many nanostructures to achieve better heating efficiency at a reduced laser power and focusing. We subsequently discuss how we harnessed the collective heating of many plasmonic nanostructures to induce strong optically controlled fluid motion, which we have called plasmonically enhanced electrothermal microfluidic flow for long-range dynamic transport of suspended particles.

RESULTS AND DISCUSSIONS

Plasmonically Enhanced Electrothermal Microfluidic Flow. The plasmonic nanostructure array was designed for enhanced absorption efficiency at a near-infrared illumination laser line of 1064 nm. Rapid particle transport is achieved by inducing electrothermal body forces in the fluid. Electrothermal flow can be optically induced by photoinduced heating and by applying an ac electric field. The heating of a fluid medium creates a temperature gradient, which results in a gradient in permittivity and electrical conductivity of the fluid. For the case of an electrode with a thin absorbing film, temperature gradients are obtained by tightly focused illumination. The application of an ac electric field acts on these inhomogeneities in the fluid and establishes an electrothermal body force on the fluid element. The expression for the average electrothermal body force per unit volume as presented by Green and coworkers[22] is given by

$$\langle f_{\mathrm{ethm}} \rangle = \frac{1}{2}\mathrm{Re}\left[\frac{\sigma\epsilon(\alpha - \beta)}{\sigma + i\omega\epsilon}(\nabla T \cdot E)E^* - \frac{1}{2}\epsilon\alpha|E|^2\nabla T\right] \quad (1)$$

where $\alpha = (1/\epsilon)(\partial\epsilon/\partial T)$, $\beta = (1/\sigma)(\partial\sigma/\partial T)$, σ and ϵ are the conductivity and permittivity of the fluid, respectively, at the angular frequency ω, and E and ∇T are the applied electric field and temperature gradient, respectively.

Metallic nanostructures have been shown to enable dramatic local heating efficiency when excited at resonance and present a way to realize nanoscale heat sources remotely controllable by light.[12] The photoinduced heating of resonantly excited plasmonic nanostructures would also result in heating of the surrounding fluid medium, establishing gradients in fluid permittivity and conductivity. By applying an ac electric field, electrothermal flow can be generated to assist in particle transport. According to the expression in eq 1, the electrothermal body force is contingent upon a strong temperature gradient, *i.e.*, the localization of the temperature field in space. Since arrays of optically excited plasmonic nanostructures can produce a large temperature rise *via* collective effects,[23−25] both enhanced heating efficiency and a higher temperature gradient could be achieved.

As the electrothermal effect requires nonuniform heating of the surrounding fluid to create temperature gradients, it is important to determine the temperature profile on the surfaces of the plasmonic nanostructure array with many thermally interacting elements. For a plasmonic nanostructure illuminated with monochromatic light, the heat power absorbed and delivered by each nanoparticle j is given by

$$Q_j = \frac{C_{abs} n \varepsilon_0 c}{2} |E_j^{ext}|^2 \quad (2)$$

where C_{abs} is the absorption cross-section of the particle, n is the refractive index of the medium, and E_j^{ext} is the external electric field experienced by the nanoparticle. For simplicity we neglect the electromagnetic interaction between nanoparticles in the array such that E_j^{ext} is the same as the electric field from the incident light E_{inc}.

The heat power delivered is then $Q_j = C_{abs} I$, where I is the intensity of the incident light and is given by

$$I = \frac{n \varepsilon_0 c}{2} |E_{inc}|^2$$

For a Gaussian illumination, the irradiance is dependent on position and in radial coordinates is given by

$$I(r) = \frac{P}{2\pi\sigma^2} e^{-r^2/2\sigma^2} \quad (3)$$

where P is the laser power and is related to the full-width at half-maximum (fwhm) of the laser beam by fwhm = $2(2 \ln 2)^{1/2}\sigma$. Thus, under Gaussian illumination, the heat power absorbed and delivered by the plasmonic nanostructures is also a function of radial coordinate.

The absorption cross-section C_{abs} of a plasmonic nanostructure was evaluated by integrating the total power dissipation density in the particle over the volume of the particle normalized by the incident intensity. This was numerically computed by finite element analysis software (COMSOL Multiphysics). Different sizes were simulated to optimize the absorption efficiency, and this was used as a figure of merit to determine the photothermal response of the nanostructures. Figure 1b shows the absorption efficiency for gold nanodisks with diameters of 200, 240, and 280 nm. For illumination at the 1064 nm laser line, the 240 nm Au disk has a higher absorption efficiency. Thus, the 240 nm Au nanodisk array is expected to result in a higher overall temperature rise. The heat power dissipation density in a 240 nm diameter gold nanodisk immersed in water and illuminated with a plane wave with electric field polarized in the z direction is shown in Figure 1a. Techniques for experimentally determining the temperature rise on plasmonic nanoparticles are not yet robust, and while some progress has been made so far,[26−30] much effort is still required in this area. Numerical evaluation of temperature rise due to many thermally interacting nanoparticles is computationally intensive. Recently Baffou *et al.*[25] showed that the temperature profile on plasmonic nanostructures in an ordered array (such as lithographically fabricated patterns used in this work) can be readily determined by taking into account the self-contribution from heat delivered by the nanoparticle plus the contribution from other nanoparticles in an array. That is, by virtue of collective heating, for any particle j the temperature rise on the surface of the particle at steady state is

$$\Delta T_j = \frac{Q_j}{4\pi k \beta r_{eq}} + \sum_{\substack{k=1 \\ k \neq j}}^{N} \frac{Q_k}{4\pi k |r_j - r_k|} \quad (4)$$

The first term on the right is the temperature rise on the surface of particle j due to self-heating power delivered by particle j. Although the power dissipation density is nonuniform as shown in Figure 1a, the temperature is uniform on the surface as well as in the volume of the nanoparticle since the thermal conductivity of the plasmonic nanostructure (gold in this case, which is 317 W/m K for the bulk) is much higher than that of the substrate and surrounding medium. The second term on the right depicts the temperature rise at the location of particle j due to the heat delivered by the other $N - 1$ particles located at a distance $|r_j - r_k|$ away, where $k = 1, 2, ..., N$. The sum of these two gives the effective temperature rise on the surface of any given nanoparticle, taking into account the effects of nearby particles.

This approach suffices to accurately model collective heating of plasmonic nanoparticles in an ordered array, as was recently experimentally verified by thermal imaging of the nanostructures using quadri-wave shearing interferometry.[25,28]

We employed a similar formalism in computing temperature rise on the surface of the nanodisks. For a

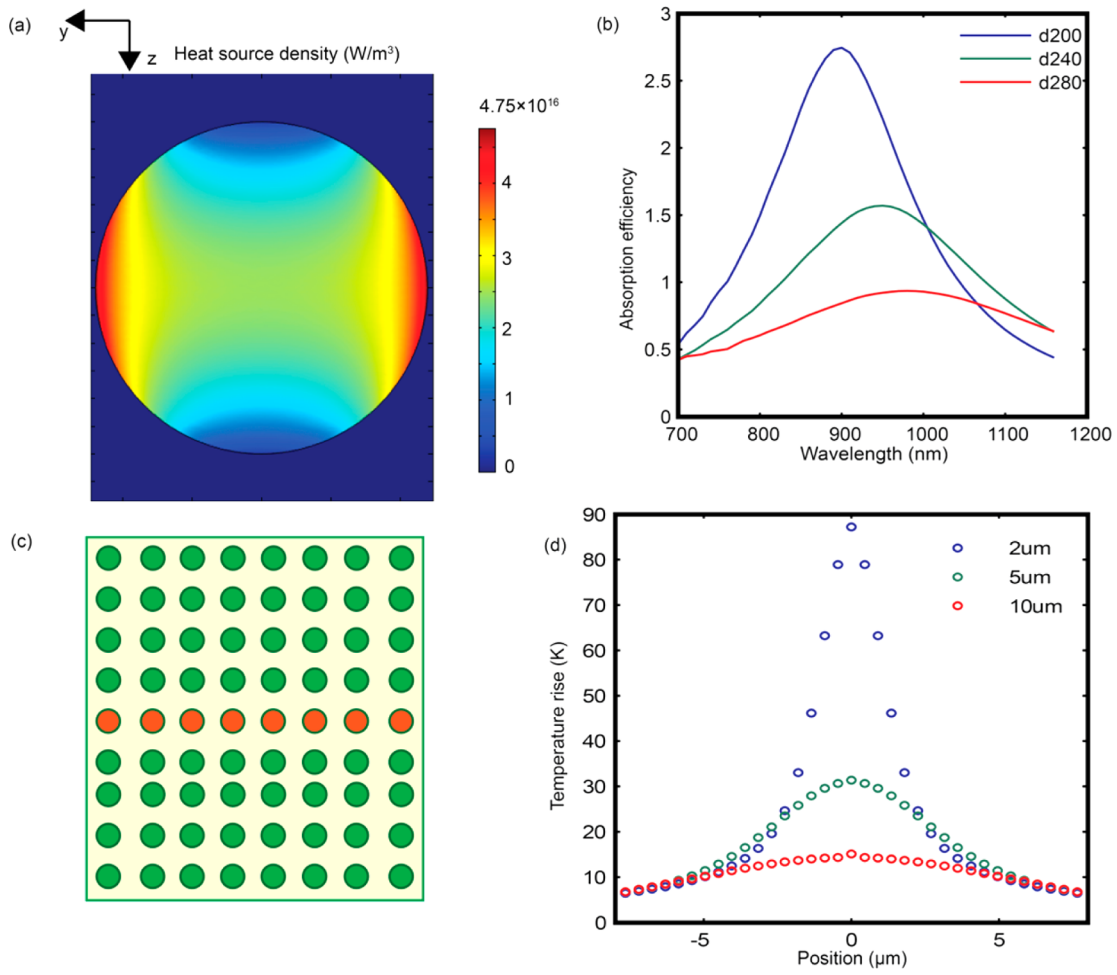

Figure 1. (a) Electromagnetic power loss density for a gold nanodisk of 240 nm diameter for an illumination intensity of 8×10^8 W/m^2; (b) absorption efficiency for 200, 240, and 280 nm gold nanodisks; (c) the line section along the middle section of the array with red particles (240 nm diameter and 450 nm lattice constant) depicting the nanoparticles whose surface temperatures were calculated while taking into account all other photostimulated particles in the square array; (d) temperature on the surface of gold nanodisks (240 nm in diameter) taken along the line depicted in (c) for beams focused to 10, 5, and 2 μm fwhm, respectively.

nanodisk with diameter D and thickness d, $\beta = \exp\{0.04 - 0.0124 \ln(D/d) + 0.0677[\ln(D/d)]^2 - 0.004\,57[\ln(D/d)]^3\}$.[31] r_{eq} is the equivalent radius of a nanosphere, whose volume is equivalent to the volume of the nanodisk, and k is the average thermal conductivity of the substrate and surrounding fluid medium. The thermal conductivity of the ITO coating is taken as 10.2 W/mK,[32] while that of the surrounding water medium was taken as 0.65 W/mK[33] for the computations.

Figure 1d shows the temperature distribution from a nanoplasmonic structure array of 240 nm gold nanodisks, for a laser power of 15 mW and focused to fwhm of 2, 5, and 10 μm calculated by using eq 4.

Note that by defoccusing the beam from a fwhm of 2 to 10 μm, the intensity decreased by a factor of 25. However, the maximum temperature rise decreased from 87 K to 15 K, a factor of only 5.8. This is because by defocusing the beam, more opticallly excited nanoscale heat sources are produced that compensate for the decreased intensity. Thus, with a defocused beam (or low intensity), it is still possible to induce a strong electrothermal effect for rapid particle transport. Additionally, even with a defocused Gaussian illumination of 10 μm fwhm, the temperature gradient along the line depicted in Figure 1c is approximately 10^6 K/m. The excitation of the nanoparticle array with a Gaussian illumination assists in generating a nonuniform temperature profile along the array surface, which is necessary for nonuniform heating of the adjoining fluid medium to establish temperature gradients as well as gradients in permittivity and conductivity. With a circular beam, with a uniform intensity distribution, such large temperature gradient along the array cannot be achieved for the same beam diameter as the Gaussian fwhm.

EXPERIMENTAL ILLUSTRATION

We subsequently demonstrate the generation of strong electrothermal fluid motion by exciting the plasmonic nanostructure arrays. Gold nanodisks of

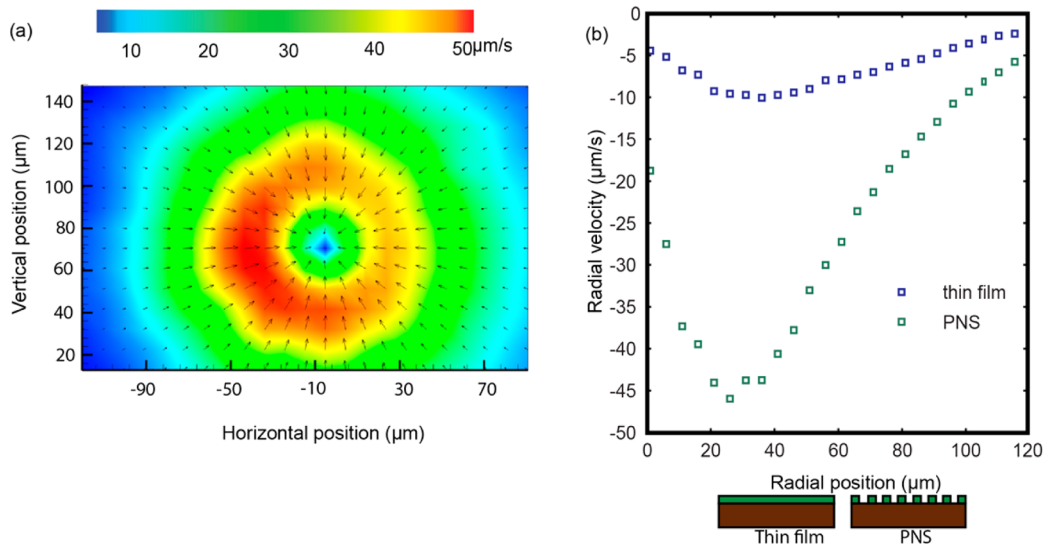

Figure 2. (a) Velocity distribution for electrothermal flow induced by the photoinduced heating of the plasmonic nanostructure array, showing the axi-symmetric flow profile. (b) Electrothermal flow for a thin film substrate and a plasmonic nanostructured substrate for the same laser power and same ac voltage of 9.8 Vpp and 100 kHz frequency.

diameter 240 nm and lattice constant of 450 nm were fabricated on an ITO-coated glass substrate using electron beam lithography. The ITO coating also serves as a conducting layer for application of external electrical signals. The details of the chip fabrication can be found in the Methods Section. Fluorescent polystyrene particles of 1 μm diameter were suspended in deionized water and manually injected into the chip. The plasmonic nanostructured substrate was illuminated with a 17 mW laser beam focused with a 40$\times$ objective lens. An external ac signal of 9.8 Vpp at 100 kHz was then applied, and immediately strong microfluidic flow was generated due to the electrothermal effect. The motion of the fluid exerts a drag force on the suspended tracer particles and transports them close to the substrate. We note that such a strong fluid and particle motion is not observed by the application of laser or electric field alone. This is because by eq 1 electrothermal fluid motion is possible only when the temperature gradient (which is achieved by photoinduced heating of the nanoparticle array) and ac electric field are simultaneously present. This plasmonically enhanced electrothermal microfluidic flow was characterized using the microparticle image velocimetry flow visualization technique.[34] The microfluidic flow field is axis-symmetric, as shown by the velocity vectors in Figure 2a obtained after particle image velocimetry (PIV) analysis of successive image frames. The vector plot shows that the electrothermal flow acts to transport suspended particles toward the central position of the laser illumination.

We also deposited a similar ITO-coated glass substrate with a thin film of gold of the same thickness as the plasmonic nanostructured substrate (PNS) to compare the strength of the electrothermal flow for both systems under similar experimental conditions. Again PIV analysis of the image frames was performed, and Figure 2b shows the angularly averaged radial velocity *versus* radial position plot for both systems for the same laser power and ac voltage of 9.8 Vpp at 100 kHz frequency.

The plasmonic nanostructure clearly shows a much stronger flow velocity with a maximum velocity of 46 μm/s in comparison to 10 μm/s for the thin film substrate. The stronger fluid velocity is attributed to the efficient photothermal heating by the PNS following the near-resonance excitation of the plasmonic nanostructures in the array. An additional possible factor is that the plasmonic nanostructures can achieve better heat localization since water in between the nanostructures has a much lower thermal conductivity, thus minimizing lateral thermal spreading along the array. On the other hand, since the thin film system is made of a continuous gold film, which has a high thermal conductivity, significant lateral heat conduction along the film would result in a lower temperature gradient along the film. Thus, much stronger flow velocity can be generated at reduced laser intensity with the PNS as compared with the thin film substrate. Experiments were also conducted with an ITO-coated glass substrate with a 100 nm ITO layer thickness, and the result showed a lower maximum velocity of about 4.6 μm/s under similar laser power and ac signal (Figure S1). Notice from Figure 2b that the electrothermal flow radial velocity from the PNS at a position 110 μm away is about 7 μm/s and increases progressively toward the illumination center. This implies that particles located over 100 μm away could be captured by the flow and rapidly accelerated toward the illuminated center. Since from eq 1 the electrothermal flow depends on the square of the ac electric field, increasing the external voltage signal increases the strength of

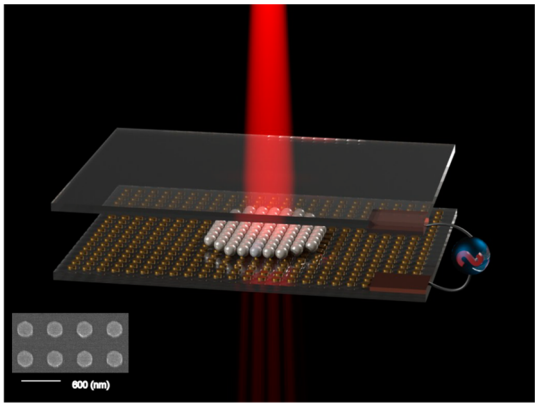

Figure 3. Illustration of the hybrid device for dynamic manipulation of particles on a plasmonic nanostructured substrate (not drawn to scale). Inset shows an SEM image of the fabricated gold nanodisk array.

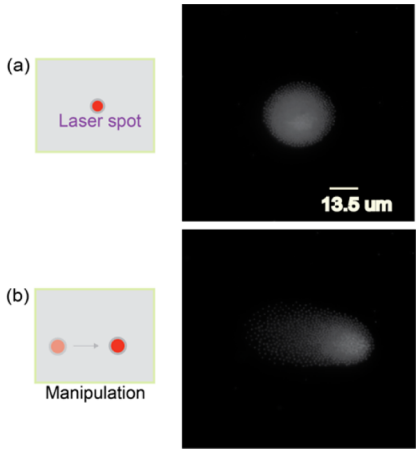

Figure 4. (a) Results showing initial capture of 1 μm particles on the PNS. (b) Moving the stage translocates the particle cluster to a new location.

the flow and even more rapid particle transport can be achieved.

We note that the plasmonically enhanced electrothermal flow above enables achieving very high transport velocities over a large spatial area in a chip in comparison with convection. The fluid transport velocity of 46 μm/s far exceeds the velocity of 1.7 μm/s achieved by Roxworthy *et al.*[35] recently based on thermoplasmonic convection. Thus, we suggest that rather than employing convection as a means of fluid transport, plasmonically enhanced electrothermal microfluidic flow presents a more efficient mechanism for rapid optofluidic control, which is highly attractive for a broad range of lab-on-a-chip applications. To our knowledge, this is the first time the electrothermal effect is being studied with respect to plasmonic systems. Previous methods of fluid and particle manipulation with plasmonic nanostructures have been based on convective transport and thermophoresis.[35−37]

Experiments were further conducted to achieve particle aggregation on the PNS. The experimental setup is similar to that used for characterizing plasmonically enhanced electrothermal microfluidic flow and is shown in Figure 3. A laser power of 17 mW was applied through a 40×, 0.6 NA objective lens, but no particle aggregation was observed under this condition. However, application of an ac voltage of 19 Vpp at 50 kHz with laser illumination resulted in the generation of electrothermal flow. The suspended 1 μm particles were continuously transported by the induced electrothermal flow, toward and away from the illuminated region, but no trapping took place. As the ac frequency was reduced from 50 kHz to 25 kHz, the suspended particles started to rapidly concentrate at the laser spot to form a large particle cluster as shown in Figure 4a. Particle trapping was achieved at the center of the illuminated region because the applied ac frequency (25 kHz) was less than the critical frequency for trapping by low-frequency electrokinetic forces.[21] When the ac electric field was turned OFF, not only did the electrothermal fluid motion cease but, in addition, the concentrated particle group was expelled from the illuminated region. We anticipated that the local field enhancement resulting from resonant excitation of the plasmonic nanostructures would establish optical gradient forces to trap the particles that are present within the illuminated region. The lack of particle trapping on turning OFF the external electric field is attributed to optically induced thermofluidic forces such as natural convection and thermophoresis that have been known to prevent stable trapping in plasmonic nanotweezers.[38]

Dynamic manipulation of the collected particle group over the PNS was achieved by translating the microscope stage from one location to another. It excites new thermal hot spots and hence electrothermal flow, which drags the particle group to the illuminated location (SI video 1). Figure 4 shows the initial position of the collected particle cluster before manipulation and the final position after manipulation to a new location. We also demonstrate the sorting of particles based on size. Both 1 and 2 μm sized particles were initially captured by illuminating the PNS and by applying an ac electric signal of 10 kHz frequency as in Figure 5a. When the ac frequency was increased from 10 kHz to 25 kHz, the initially captured 2 μm particles were expelled from the aggregation, while the 1 μm particles still remained as shown in Figure 5b. This size-dependent sorting based on applied ac frequency is attributed to the frequency-dependent polarization of the particle electrical double layer. The relaxation frequency for this polarization mechanism scales as the square of the particle radius, which results in a critical frequency for particle trapping by REP that scales as the square of the particle radius.[21] Above the critical frequency, a trapped particle is released from the trap.

In order to ascertain whether the collective heating with the nanoparticle array could enable rapid

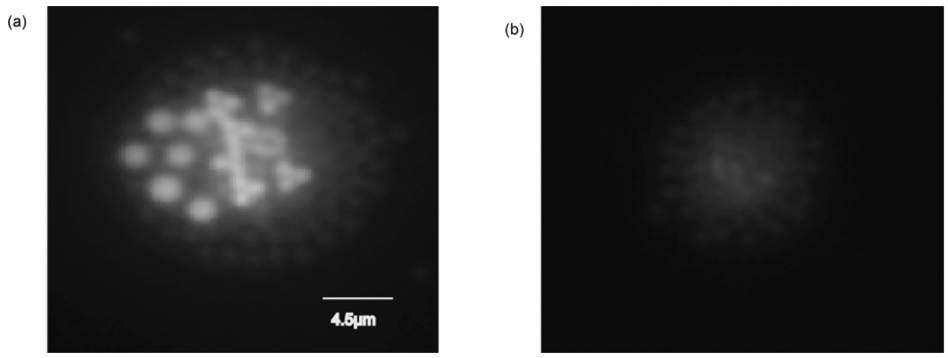

Figure 5. Separation of 1 μm from 2 μm particles. (a) Both particles were initially captured at 10 kHz frequency. (b) At 25 kHz frequency, only the 1 μm particles remain captured, while the 2 μm particles are expelled from the trap.

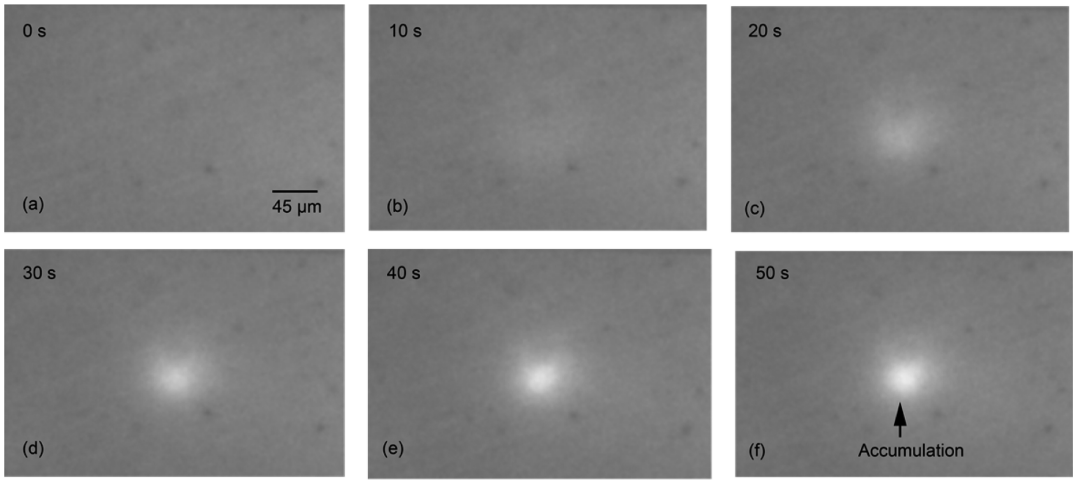

Figure 6. Concentration of 100 nm polystyrene particles on the PNS, when a 17 mW laser and a 19 Vpp ac electric field of 50 kHz frequency were applied. Frames a−f show the evolution of the aggregation with time.

concentration of nanoparticles under low illumination intensity, experiments were conducted with a 17 mW loosely focused laser beam with a 10× objective lens (0.25 NA). For this experiment, 100 nm polystyrene particles were used in order to ascertain if high-throughput concentration of particles at this length scale can be achieved with the PNS. With either an ac electric field or laser illumination applied, no particle concentration was observed. However, rapid particle concentration was observed when an ac voltage of 19 Vpp at 50 kHz frequency was applied with the laser excitation, as shown in Figure 6 and the Supporting Information (SI video 2).

Thus, the PNS eliminates the requirement for highly focused illumination to drive particle transport and aggregation. This ability to achieve rapid particle concentration on the PNS with loosely focused optical illumination would benefit applications requiring handling of biological particles in high-throughput mode with minimal risk of optical damage.

Accelerated Particle Capture beyond Brownian Diffusion. Rapid particle transport and concentration is very critical for several applications. Here we quantify the rapid concentration of particles in comparison with diffusion-limited transport. A key issue limiting the performance of biosensors including plasmonic sensors is diffusion-limited transport of analytes. Here we suggest a means to fish out particles from hundreds of micrometers away in a dilute solution and rapidly concentrate them to one spot on the PNS. For this purpose, a dilute solution of 1 μm fluorescent polystyrene beads was prepared by diluting the original solution to 10^7 particles per milliliter. The particles were manually injected into the chip. When only laser illumination was applied on the chip, no particle capture was observed, even after 10 min. On applying an ac signal of 21 Vpp amplitude at 10 kHz frequency, an electrothermal flow was generated and particles several micrometers away were rapidly transported toward the illuminated area of the PNS. The rapid particle transport was compared with free diffusion. The trajectories of five 1 μm particles, which were transported from distances ranging from 130 to 220 μm away, were monitored, and it was observed that, on average, the particles were trapped in less than 12 s. We estimated how long it will take a particle to cover a distance of 200 μm if it was allowed to freely diffuse under Brownian motion. The mean square

diffusion distance is given by $R^2(t) = 2Dt$, and the diffusion coefficient $D = k_BT/3_{\pi\eta d}$, where D, k_B, d, and η are the diffusion coefficient, Boltzmann constant, diameter of the sphere, and viscosity of the medium, respectively.

At a temperature of 353 K, the viscosity of water $\eta = 3.55 \times 10^{-4}$ Pa[39] was used to compute the diffusion coefficient of 1.35 μm^2/s. It would take over 4 h for a 1 μm particle to diffuse through this distance by free diffusion, which would limit the response time of plasmonic biosensors. Our approach enables over 3 orders of magnitude faster transport and concentration of particles on the PNS and would improve the response time of LSPR biosensors and enable other lab-on-a-chip applications. In addition, our approach also enables faster concentration with speed well exceeding that obtainable by using plasmonic optical latices.[40]

CONCLUSION

We have proposed plasmonically enhanced electrothermal microfluidic flow as an alternative approach for light-driven fluid motion in plasmonic-based optofluidic systems and demonstrated fluid velocities over 45 μm/s. This fluid motion mechanism requires the simultaneous presence of both light-induced heating of the plasmonic nanostructures and an ac electric field. Furthermore, we have harnessed the collective heating of plasmonic nanoparticles excited at near-resonance to achieve dynamic manipulation, sorting, translation, and patterning of micro- and nanoscale particles. The approach clearly shows particle trapping and manipulation driven by nonradiative energy decay from photoexcited nanoparticle array. Additionally, we have also demonstrated concentration of nanoscale objects with loosely focused illumination with a 10×, 0.25 NA objective. Due to the low optical intensity, this scheme drastically reduces the risk of optical damage or opticution. This approach of particle concentration and sorting on a PNS is very robust and insensitive to laser intensity variation, unlike other designs relying on thermofluidic forces whereby a variation of laser intensity above the threshold causes instability in particle trapping.[10,37] Our approach is ideally suited for biosensing applications due to the ability to rapidly sort and concentrate particles on a plasmonic substrate, where the optical hot spots generated by excitation of the plasmonic nanostructures could be used for biological sensing. Our work reveals that the local heating effect following resonant excitation of plasmonic nanoparticles is not deleterious for particle trapping applications as have been portrayed in the literature. We envision that this technique would be of benefit for a wide range of applications including biosensing and surface-enhanced spectroscopies.

METHODS SECTION

Chip Fabrication. Gold nanodisks of 240 nm diameter were fabricated on an ITO-coated glass substrate (surface resistivity of 500 ohm/sq) using electron beam lithography (EBL). Approximately 120 nm of ZEP-520A resist was spin-coated on the ITO-coated glass substrate. After EBL writing, the resist was developed for 2 min in ZED N50, rinsed with isopropyl alcohol (IPA), and dried under nitrogen. A 3 nm titanium film adhesion layer followed by a 30 nm gold film was deposited in an electron beam evaporation chamber. Metal lift-off was carried out by soaking in ZDMAC for 20 min, after which the chip was rinsed in IPA. A microfluidic chamber was sandwiched between the electrode (with the EBL patterns) and another electrode made of unpatterned ITO-coated glass. The microfluidic chamber was made from 90 μm thick double-sided adhesive tape, with the EBL patterns well within the chamber. Electrical contacts were made for application of an ac electric field on the ITO-coated side of the substrates using adhesive copper tapes.

Illumination System and Imaging. Visualization of the particles was accomplished using an inverted Nikon TE2000U microscope equipped with a Nikon objective lens (40× and 10×). The excitation beam from a CW Nd:YVO_4 laser operating at 1064 nm was also passed through the same objective.

MicroPIV Analysis. For PIV analysis, 1 μm red fluorescent polystyrene particles were used as tracer particles. The particles were dispersed in deionized water and introduced into the chip. Images were acquired with a PCO camera. For experiments with a plasmonic nanostructured substrate, the frame rate was 13 frames per second, while for the equivalent thin film design, the frame rate was 10 frames per second. The Enhanced Digital Particle Image Velocimetry (EDPIV) software package was used for the Micro-PIV analysis. At least 1500 images were collected and analyzed.

Simulation. The computational domain spans 9000 nm along the direction of propagation (x-axis) and 450 nm along y and z directions. Perfectly matched layers (PML) are placed at the top and bottom of the domain to prevent backscatter from the boundaries. The plane wave was generated by a time harmonic surface current positioned just below the upper PML in the yz-plane. In order to ensure normal incidence of the fields and mimic a two-dimensional array of nanodisks, perfect electric and perfect magnetic conductor boundary conditions were used. The absorption cross-section was computed by integrating the electromagnetic power loss density over the volume of the nanodisk and dividing the result by the incident intensity. The absorption efficiency was obtained as the absorption cross-section normalized by the geometrical cross-sectional area.

Conflict of Interest: The authors declare no competing financial interest.

Acknowledgment. The authors acknowledge financial support from NSF MRSEC Grant DMR-1120923. J.N. also acknowledges financial support from Purdue Calumet Water Institute.

Supporting Information Available: Videos showing concentration and manipulation of micro- and nanoscale particles. Experimentally measured radial velocity for electrothermal flow using a 100 nm thick ITO coating on a glass substrate. Dimensional analysis of the heat equation. This material is available free of charge *via* the Internet at http://pubs.acs.org.

REFERENCES AND NOTES

1. Ashkin, A. Optical Trapping and Manipulation of Neutral Particles Using Lasers. *Proc. Natl. Acad. Sci. U.S.A.* **1997**, *94*, 4853–4860.
2. Neuman, K. C.; Block, S. M. Optical Trapping. *Rev. Sci. Instrum.* **2004**, *75*, 2787–2809.
3. Kang, J.-H.; Kim, K.; Ee, H.-S.; Lee, Y.-H.; Yoon, T.-Y.; Seo, M.-K.; Park, H.-G. Low-Power Nano-Optical Vortex Trapping

via Plasmonic Diabolo Nanoantennas. *Nat. Commun.* **2011**, *2*, 582.
4. Grigorenko, a. N.; Roberts, N. W.; Dickinson, M. R.; Zhang, Y. Nanometric Optical Tweezers Based on Nanostructured Substrates. *Nat. Photonics* **2008**, *2*, 365–370.
5. Tsai, W.; Huang, J.; Huang, C. Selective Trapping or Rotation of Isotropic Dielectric Microparticles by Optical Near Field in a Plasmonic Archimedes Spiral. *Nano Lett.* **2014**, *14*, 547–552.
6. Wang, K.; Schonbrun, E.; Steinvurzel, P.; Crozier, K. B. Trapping and Rotating Nanoparticles Using a Plasmonic Nano-Tweezer with an Integrated Heat Sink. *Nat. Commun.* **2011**, *2*, 469.
7. Tanaka, Y.; Kaneda, S.; Sasaki, K. Nanostructured Potential of Optical Trapping Using a Plasmonic Nanoblock Pair. *Nano Lett.* **2013**, *13*, 2146–2150.
8. Baffou, G.; Quidant, R.; Girard, C. Heat Generation in Plasmonic Nanostructures: Influence of Morphology. *Appl. Phys. Lett.* **2009**, *153109*, 4–7.
9. Govorov, A. O.; Richardson, H. H. Generating Heat with Metal Nanoparticles. *Nano Today* **2007**, *2*, 30–38.
10. Roxworthy, B. J.; Ko, K. D.; Kumar, A.; Fung, K. H.; Chow, E. K. C.; Liu, G. L.; Fang, N. X.; Toussaint, K. C. Application of Plasmonic Bowtie Nanoantenna Arrays for Optical Trapping, Stacking, and Sorting. *Nano Lett.* **2012**, *12*, 796–801.
11. Neumann, O.; Urban, A. S.; Day, J.; Lal, S.; Nordlander, P.; Halas, N. J. Solar Vapor Generation Enabled by Nanoparticles. *ACS Nano* **2013**, *7*, 42–49.
12. Baffou, G.; Quidant, R. Thermo-plasmonics: Using Metallic Nanostructures as Nano-sources of Heat. *Laser Photonics Rev.* **2013**, *187*, 171–187.
13. Saleh, A. A. E.; Dionne, J. A. Toward Efficient Optical Trapping of Sub-10-nm Particles with Coaxial Plasmonic Apertures. *Nano Lett.* **2012**, *12*, 5581–5586.
14. Huidobro, P. A.; Ota, S.; Yang, X.; Yin, X.; Garcia-Vidal, F. J.; Zhang, X. Plasmonic Brownian Ratchet. *Phys. Rev. B: Condens. Matter Mater. Phys.* **2013**, *88*, 201401.
15. Cinel, N. A.; Bütün, S.; Özbay, E. Electron Beam Lithography Designed Silver Nano-Disks Used as Label Free Nano-Biosensors Based on Localized Surface Plasmon Resonance. *Opt. Express* **2012**, *20*, 2587–2597.
16. Piliarik, M.; Sípová, H.; Kvasnička, P.; Galler, N.; Krenn, J. R.; Homola, J. High-Resolution Biosensor Based on Localized Surface Plasmons. *Opt. Express* **2012**, *20*, 672–680.
17. Walter, A.; März, A.; Schumacher, W.; Rösch, P.; Popp, J. Towards a Fast, High Specific and Reliable Discrimination of Bacteria on Strain Level by Means of SERS in a Microfluidic Device. *Lab Chip* **2011**, *11*, 1013–1021.
18. Fan, X.; White, I. M. Optofluidic Microsystems for Chemical and Biological Analysis. *Nat. Photonics* **2011**, *5*, 591–597.
19. Juan, M. L.; Righini, M.; Quidant, R. Plasmon Nano-Optical Tweezers. *Nat. Photonics* **2011**, *5*, 349–356.
20. Williams, S. J.; Kumar, A.; Wereley, S. T. Electrokinetic Patterning of Colloidal Particles with Optical Landscapes. *Lab Chip* **2008**, *8*, 1879–1882.
21. Kumar, A.; Kwon, J. S.; Williams, S. J.; Green, N. G.; Yip, N. K.; Wereley, S. T. Optically Modulated Electrokinetic Manipulation and Concentration of Colloidal Particles near an Electrode Surface. *Langmuir* **2010**, *26*, 5262–5272.
22. Ramos, A.; Morgan, H.; Green, N. G.; Castellanos, A. Ac Electrokinetics: A Review of Forces in Microelectrode Structures. *J. Phys. D: Appl. Phys.* **1998**, *31*, 2338–2353.
23. Richardson, H. H.; Carlson, M. T.; Tandler, P. J.; Hernandez, P.; Govorov, A. O. Experimental and Theoretical Studies of Light-to-Heat Conversion and Collective Heating Effects in Metal Nanoparticle Solutions. *Nano Lett.* **2009**, *9*, 1139–1146.
24. Keblinski, P.; Cahill, D. G.; Bodapati, A.; Sullivan, C. R.; Taton, T. A. Limits of Localized Heating by Electromagnetically Excited Nanoparticles. *J. Appl. Phys.* **2006**, *100*, 054305.
25. Baffou, G.; Berto, P.; Esteban, B. U.; Quidant, R.; Monneret, S.; Polleux, J.; Rigneault, H. Photoinduced Heating of Nanoparticle Arrays. *ACS Nano* **2013**, *7*, 6478–6488.
26. Baffou, G.; Kreuzer, M. P.; Kulzer, F.; Quidant, R. Temperature Mapping near Plasmonic Nanostructures Using Fluorescence Polarization Anisotropy. *Opt. Express* **2009**, *17*, 3291–3298.
27. Carlson, M. T.; Khan, A.; Richardson, H. H. Local Temperature Determination of Optically Excited Nanoparticles and Nanodots. *Nano Lett.* **2011**, *11*, 1061–1069.
28. Baffou, G.; Bon, P.; Savatier, J.; Polleux, J.; Zhu, M.; Merlin, M.; Rigneault, H.; Monneret, S. Thermal Imaging of Nanostructures by Quantitative Optical Phase Analysis. *ACS Nano* **2012**, *6*, 2452–2458.
29. Coppens, Z. J.; Li, W.; Walker, D. G.; Valentine, J. G. Probing and Controlling Photothermal Heat Generation in Plasmonic Nanostructures. *Nano Lett.* **2013**, *13*, 1023–1028.
30. Yamauchi, H.; Ito, S.; Yoshida, K.; Itoh, T.; Tsuboi, Y.; Kitamura, N.; Miyasaka, H. Temperature near Gold Nanoparticles under Photoexcitation: Evaluation Using a Fluorescence Correlation Technique. *J. Phys. Chem. C* **2013**, *117*, 8388–8396.
31. Baffou, G.; Quidant, R.; García de Abajo, F. J. Nanoscale Control of Optical Heating in Complex Plasmonic Systems. *ACS Nano* **2010**, *4*, 709–716.
32. Hohnholz, D.; Schweikart, K.-H.; Hanack, M. A Simple Method for the Subdivision of ITO Glass Substrates. *Adv. Mater.* **1999**, *11*, 646–649.
33. Ramires, M. L. V.; Nieto de Castro, C. A.; Nagasaka, Y.; Nagashima, A.; Assael, M. J.; Wakeham, W. A. Standard Reference Data for the Thermal Conductivity of Water. *J. Phys. Chem. Ref. Data* **1995**, *24*, 1377.
34. Santiago, J. G.; Wereley, S. T.; Meinhart, C. D.; Beebe, D. J.; Adrian, R. J. A Particle Image Velocimetry System for Microfluidics. *Exp. Fluids* **1998**, *25*, 316–319.
35. Roxworthy, B. J.; Bhuiya, A. M.; Vanka, S. P.; Toussaint, K. C. Understanding and Controlling Plasmon-Induced Convection. *Nat. Commun.* **2014**, *5*, 3173.
36. Donner, J. S.; Baffou, G.; McCloskey, D.; Quidant, R. Plasmon-Assisted Optofluidics. *ACS Nano* **2011**, *5*, 5457–5462.
37. Shoji, T.; Shibata, M.; Kitamura, N.; Nagasawa, F.; Takase, M.; Murakoshi, K.; Nobuhiro, A.; Mizumoto, Y.; Ishihara, H.; Tsuboi, Y. Reversible Photoinduced Formation and Manipulation of a Two-Dimensional Closely Packed Assembly of Polystyrene Nanospheres on a Metallic Nanostructure. *J. Phys. Chem. C* **2013**, *117*, 2500–2506.
38. Ploschner, M.; Mazilu, M.; Krauss, T.; Dholakia, K. Optical Forces near a Nanoantenna. *J. Nanophotonics* **2010**, *4*, 041570.
39. Kestin, J.; Sokolov, M.; Wakeham, W. A. Viscosity of Liquid Water in the Range −8 to 150 °C. *J. Phys. Chem. Ref. Data* **1978**, *7*, 941.
40. Chen, K.; Lee, A.; Hung, C.; Huang, J.; Yang, Y. Transport and Trapping in Two-Dimensional Nanoscale Plasmonic Optical Lattice. *Nano Lett.* **2013**, *13*, 4118–4122.